

THESIS

EMPIRICAL COMPARISON OF NEUTRON ACTIVATION
SAMPLE ANALYSIS METHODS

Submitted by

Elizabeth Gillenwalters

Department of Environmental and Radiological Health Sciences

In partial fulfillment of the requirements

For the degree of Master of Science

Colorado State University

Fort Collins, Colorado

Spring 2011

Master's Committee:

Advisor: Thomas Johnson

John Pinder

Phil Kearney

ABSTRACT

EMPIRICAL COMPARISON OF NEUTRON ACTIVATION
SAMPLE ANALYSIS METHODS

The U.S. Geological Survey (USGS) operates a research reactor used mainly for neutron activation of samples, which are then shipped to industrial customers. Accurate nuclide identification and activity determination are crucial to remain in compliance with Code of Federal Regulations guidelines. This facility utilized a Canberra high purity germanium detector (HPGe) coupled with Canberra Genie™ 2000 (G2K) software for gamma spectroscopy.

This study analyzed the current method of nuclide identification and activity determination of neutron activated materials utilized by the USGS reactor staff and made recommendations to improve the method. Additionally, analysis of attenuators, effect of detector dead time on nuclide identification, and validity of activity determination assumptions were investigated.

The current method of activity determination utilized the G2K software to obtain ratio of activity per nuclide identified. This determination was performed without the use of geometrically appropriate efficiency calibration curves. The ratio of activity per nuclide was used in conjunction with an overall exposure rate in mR/h obtained via a Fluke Biomedical hand-held ion chamber. The overall exposure rate was divided into

individual nuclide amounts based on the G2K nuclide ratios. A gamma energy of 1 MeV and a gamma yield of 100% was assumed for all samples. Utilizing the gamma assumption and nuclide ratios, a calculation was performed to determine total sample activity in μCi (microCuries).

An alternative method was proposed, which would eliminate the use of exposure rate and rely solely on the G2K software capabilities. The G2K software was energy and efficiency calibrated with efficiency curves developed for multiple geometries. The USGS reactor staff were trained to load appropriate calibration data into the G2K software prior to sample analysis.

Comparison of the current method and proposed method demonstrated that the activity value calculated with the 1 MeV assumption could be as much as 3-4 orders of magnitude higher than the activity value established with the G2K software. The exposure rate calculation was also performed for each sample using actual gamma energies and yields to verify accuracy of the G2K software calibration.

Facility specifications for detector dead time during sample analysis were stated to be 10% or less. Investigation of the effect of detector dead time on nuclide identification was performed. It was demonstrated that accurate nuclide identification could be performed with a detector dead time as high as 86.08% and a keV tolerance range of 1.5. A shielded lead cave was created to allow for greater source-to-detector distance. Additionally, an attenuator system was developed to aid in the reduction of detector dead time to meet facility specifications of less than 10%.

Acknowledgements

I would like to thank Drs. Thomas Johnson, John Pinder, and Phil Kearney for being dedicated to my project. Your knowledge and experience have been invaluable to me throughout this endeavor.

My graduate education was funded by a fellowship from NIOSH Mountain and Plains Education and Research Center, for which I am eternally grateful.

My warmest gratitude goes to Tim Debey and the TRIGA reactor staff at the U.S. Geological Survey in Denver for allowing me the opportunity to work alongside them throughout the summer of 2010.

To my husband and children, thank you for allowing me the opportunity to follow my dreams. Hopefully all the time spent away from home and late nights spent studying will pay off in the end!

Contents

Abstract of Thesis	ii
Acknowledgements	iv
List of Tables	vii
List of Figures	viii
List of Abbreviations	ix
1 Introduction and Background	1
1.1 Neutron Activation	1
1.2 Geological Survey TRIGA Reactor	1
1.3 Radioactive Materials Shipment	2
1.4 Dead Time	2
1.5 Coincidence Summing	3
1.6 Objective	3
2 Materials and Methods	6
2.1 Standards	6
2.2 HPGe	7
2.3 HPGe Calibration	9
2.4 Detector Dead Time	11
2.5 Attenuators	11
2.6 Current Method of Activity Determination	12
2.7 Proposed Method of Activity Determination	13
3 Results	15
3.1 Efficiency Curves	15
3.2 Dead Time Analysis	15
3.3 Attenuation Coefficients	17
3.4 Comparison Using Various Attenuators	17
3.5 Method Comparison	18
3.6 Further Testing of Equation 2.4 Validity	21
4 Conclusion	25
4.1 Attenuators and Efficiency	25
4.2 Detector Dead Time	25
4.3 Method Comparison	26
4.4 Further Studies	26

Bibliography	27
Appendix A: Photos	29
Appendix B: Derivation of Equation 2.4	31
Appendix C: Background	32
Appendix D: USGS Shipment Data	37

List of Tables

1.1	49 CFR Part 172-173: External radiation standards for all packages	5
1.2	10 CFR Part 71.47: Rules for exclusive use shipments	5
2.1	Ten major photopeaks of Eu-152	7
2.2	Canberra detector specifications	8
2.3	Efficiency calibration configurations	10
3.1	NaOH experiment	22
3.2	Equation 2.4 values obtained for Eu-152 standard	24
3.3	Genie values obtained using Eu-152 standard	24
D.1	USGS shipment data	38

List of Figures

1.1	Graph of dead time vs. resolving time	3
2.1	Schematic of germanium detector	8
2.2	Photograph of detector	9
2.3	Detector dimensions	9
2.4	Eu-152 spectrum	9
3.1	Efficiency curve for Eu-152 standard centered on 0.5 cm spacer.	15
3.2	Efficiency curve for Eu-152 standard centered on 5.5 cm spacer	16
3.3	Efficiency curve for Eu-152 standard in position %A1	16
3.4	Comparison of identified peaks at various dead-times	17
3.5	Comparison of lead attenuation coefficients	18
3.6	Comparison of water attenuation coefficients	18
3.7	Efficiency curves for Eu-152 standard.	19
3.8	Efficiency curves for Eu-152 standard in small type A shipping can.	19
3.9	Shipments containing Na-24 ($En=1$ assumption)	20
3.10	Log-log graph of Na-24 effect on G2K value	20
3.11	Shipments not containing Na-24 ($En=1$ assumption)	21
3.12	Shipments containing Na-24 (no En assumption)	21
3.13	Shipments not containing Na-24 (no En assumption)	22
A.1	Detector inside shielding	29
A.2	Shielding with lid open	29
A.3	Eu-152 sealed sources	29
A.4	Small type A shipping can	29
A.5	Lead attenuator	30
A.6	Water Marinelli attenuator	30
A.7	Inner view of lead cave	30
A.8	Position \$A2	30
C.1	Graph of gamma-ray interactions	33
C.2	Schematic of photoelectric effect	34
C.3	Schematic of Compton scattering	34
C.4	Schematic of pair production	36

List of Abbreviations

ALARA	as low as reasonably achievable
Bq	becquerel
C	Coulomb
cc	cubic centimeter
CFR	Code of Federal Regulations
Ci	Curie
cps	counts per second
dps	decays per second
FWHM	full width half max
g	gram
G2K	Genie™ 2000 Spectroscopy
GSTR	Geological Survey TRIGA Reactor
h	hour
HPGe	high purity germanium
in.	inches
J	Joule
keV	kiloelectron volt
L	liter
MBq	megabecquerel
MeV	megaelectron volt
mm	millimeter
mrem	millirem
mSv	milliSievert
MW	megawatt
NIST	National Institute of Standards and Technology
R	Roentgen
s	seconds
USGS	U.S. Geological Survey
VDC	Volts direct current
μCi	microCurie

CHAPTER 1

Introduction and Background

1.1 Neutron Activation

Neutron activation is defined as when a stable material is placed into a neutron radiation field, such as that generated by a nuclear reactor for the purpose of activating atoms. Neutrons are captured by atoms in the irradiated material causing those materials to become unstable radioactive isotopes, which then emit alpha, beta, and/or gamma-rays. These materials are analyzed utilizing gamma spectroscopy, which utilizes the measurement of emitted gamma-rays via a semiconductor detector. The rate of gamma-ray emission as well as the distinct energy of those gamma-rays allows for identification of individual radionuclides within a sample (USGS, 2005).

1.2 Geological Survey TRIGA Reactor

The U.S. Geological Survey operates a research reactor used for neutron activation. The GSTR (Geological Survey TRIGA Mark 1 reactor) is a 1 MW (megawatt) swimming-pool type reactor using uranium/zirconium hydride fuel. The maximum neutron flux is 3×10^{13} neutrons per square centimeter-second (USGS, 2005).

1.3 Radioactive Materials Shipment

Neutron activation materials from the GSTR are shipped to industrial customers. Some examples of the isotopes contained in these activated materials include Ar-41, Ba-133, Cd-109, Mn-54, Na-24 and Zn-65. These shipments must comply with CFR (Code of Federal Regulations) guidelines as listed in Tables 1.1, 1.2.

To remain in compliance with the CFR, accurate nuclide identification and activity determination is crucial. Due to the short lived nature of many of the neutron activation samples, it is important to ship these samples quickly as well as accurately assay the contents.

1.4 Dead Time

Neutron identification via gamma spectroscopy can be limited by dead time, which as defined by Gollnick is the minimum time lapse between two ionizing events occurring in the counter such that they are individually distinguished. Gollnick's definition is based solely on the counter's ability to record separate events and is independent of the electronic circuitry associated with the counter setup. Dead time becomes a problem when the activated samples of high radioactivity are placed close to the detector. High dead times can cause shifting of the full photopeak, resulting in misidentification of radioactive isotopes.

The dead time as defined by Canberra for the Genie software (G2K) is 'The time that the instrument is busy processing an input signal and is not able to accept another input; often expressed as a percentage' (Canberra, 2010). The Canberra definition of dead time is actually describing resolving time, which is defined by Gollnick as the minimum time lapse required for the electronics connected to the detector to reset from the first event and be able to detect the second event. The resolving time is slightly longer than dead time as the resolving time allows time for the second pulse to

be large enough to cause the electronics to register a second event (Fig. 1.1) (Gollnick, 2004). Resolving time will be referred to as detector dead time for the purpose of this paper.

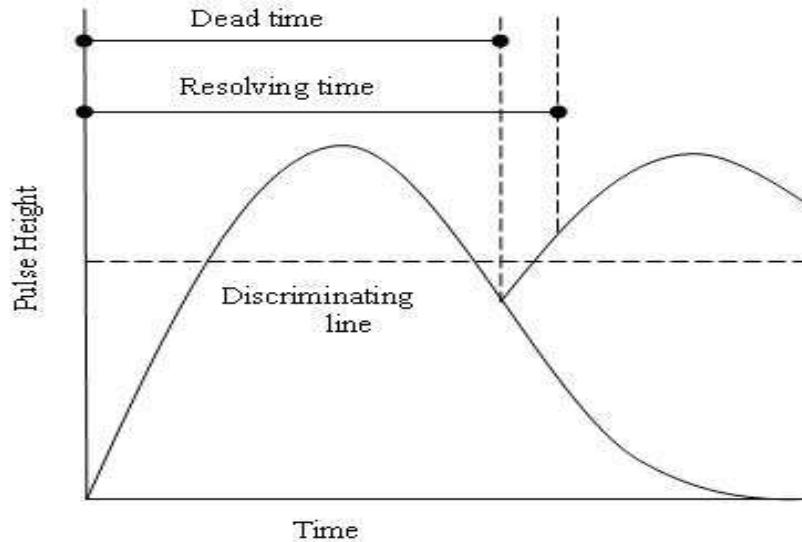


Figure 1.1: Graph of dead time vs. resolving time

1.5 Coincidence Summing

Coincidence summing occurs with radionuclides that emit two or more cascading photons within the resolving time of the detector (Debertin and Schötzig, 1979). The result of coincidence summing is a loss of counts from the full energy peak leading to lower detection efficiency. Summing effects depend heavily on the square of the detector solid angle and can be minimized by reducing the solid angle, i.e. increasing source-to-detector distance (Knoll, 2000). Geometries closer than 100 mm (millimeters) (3.94 in.(inches)) can result in an error of 20-40% (Debertin et al., 1979).

1.6 Objective

The objective of this study was multifaceted. The overall objective was to improve the current method for nuclide identification and activity determination of activated

materials utilized by the GSTR staff. The current method of activity determination was not using the G2K software to its fullest potential and was also relying on several assumptions for activity determination. The proposed method removes the reliance on assumptions, thereby allowing for more accurate identification of shipped materials and individual radionuclide activity. The goal was met by development of a set of efficiency curves with the G2K software, giving accurate activity determination for a full set of sample geometries.

Several other issues underlying the overall objective were also investigated. The validity of a long-standing health physics rule of thumb was investigated for use in neutron activation sample analysis. Additionally, the effect of detector dead-time on accurate nuclide identification by the G2K software was investigated.

Table 1.1: 49 CFR Part 172-173: External radiation standards for all packages

Dose Range	Location	Shipment Type
0 - 2 mSv/h	Any point on external surface	Normal conditions
2 - 10 mSv/h	Any point outer surface of vehicle	Exclusive use
0 - 0.1 mSv/h	Any point 2 meters (80 in.) from outer lateral surface of vehicle	Exclusive use
0 - 0.02 mSv/h	Any normally occupied space unless personnel comply with 10 CFR 20.1502	Exclusive use

Table 1.2: 10 CFR Part 71.47: Rules for exclusive use shipments

Shipment must be made in closed transport vehicle
Package must be secured within the vehicle in a fixed position during transportation
No loading or unloading operations between beginning and end of transportation
Shipper must provide specific written instructions for maintenance of the exclusive use shipments controls

mSv/h (milliSievert per hour)

CHAPTER 2

Materials and Methods

2.1 Standards

Eu-152 NIST (National Institute of Standards and Technology) traceable sealed disk standards were used for energy calibration of the HPGe (high purity germanium) detector utilized for this study (Fig. A.3). Eu-152 was chosen as the calibration standard as it produces a wide range of gamma energies, with four photopeaks having decay probabilities greater than 10% and three photopeaks having decay probabilities greater than 20%. These seven photopeaks, listed in Table 2.1, cover an energy range of 121.78 to 1407.95 keV (kiloelectron volt). It also has a relatively long half life of 13.52 years.

$$A = A_0 e^{-\lambda t} \quad (2.1)$$

where A = decay corrected activity (Bq (becquerel))

A_0 = initial activity (Bq)

λ = decay constant (Eq. 2.2)

t = time since initial activity.

$$\lambda = \frac{\text{Ln}(2)}{T_{1/2}} \quad (2.2)$$

Table 2.1: Ten major photopeaks of Eu-152

Photopeak energy (keV)	Probability of Decay
121.78	28.4 %
344.27	26.5 %
367.71	0.9 %
443.98	2.8 %
778.89	12.7 %
867.32	4.2 %
964.01	14.4 %
1085.80	10.0 %
1112.00	13.3 %
1212.80	1.4 %
1407.95	20.7 %

where $\lambda =$ decay constant (t^{-1})

$T_{1/2} =$ radionuclide half life(t).

Duplicate Eu-152 standards with three activities of 1.8×10^4 Bq (0.484 μ Ci (microCuries)), 3.4×10^4 Bq (0.907 μ Ci), and 3.6×10^4 Bq (0.961 μ Ci), were utilized individually as well as in various combinations. All three standards were created on 5 March 2010 and were decay corrected according to Eq. 2.1. The total decay of the Eu-152 standards from their creation to the end of this study was less than 2% of the initial activity.

2.2 HPGe

A high purity germanium closed-end coaxial Canberra detector was utilized for all gamma spectroscopy procedures (Figs. 2.2, 2.3). The detector and software specifications available from the manufacturer are outlined in Table 2.2.

The detector was surrounded by 101.6 mm (4 in.) of lead lined with a thin layer of copper, approximately 2 mm (0.08 in.), on all four sides (Fig. A.1). A rolling lid identical in structure was used to enclose the detector when sample size allowed (Fig. A.2). Measurements were made to indicate where the detector axis intersected

Table 2.2: Canberra detector specifications

HPGe Specifications and Components
Detector Model GC1418, Serial Number 9892187
Cryostat Model 7500
Preamplifier Model 2002C
High voltage setting: 4500 VDC
Resolution: 1.8 keV (FWHM) at 1.33 MeV (megaelectron volt)
Active volume: 61.3 cc (cubic centimeter) [Fig. 2.3]
14% relative efficiency
Canberra Genie™ 2000 Gamma Spectroscopy Software, V3.1a
Canberra Model 2026 amplifier, Model 8701 ADC , Multiport II electronics

with the lid with the lid in the fully closed position. This allowed for point source geometry.

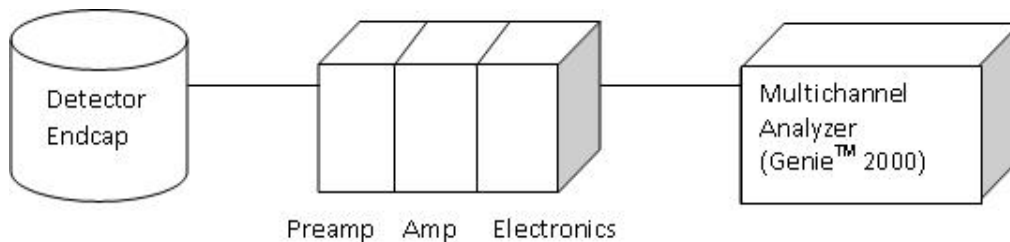


Figure 2.1: Schematic of germanium detector

The lead was removed from the lid in the previously determined location of the detector axis. This allowed placement of samples into a well directly on the axis of the detector. A lead “cave” lined with copper was built on the lid to surround the well, which allows for shielding of any workers in the detector room (Figs. A.2, A.7). The lead “cave” also contains shelves allowing for attenuators to be placed between the sample and the detector (Fig. A.7). The lead cave was developed to allow for increased source-to-detector distance for inverse square reduction of higher activity samples while maintaining direct alignment with the axis of the detector.



Figure 2.2: Photograph of detector

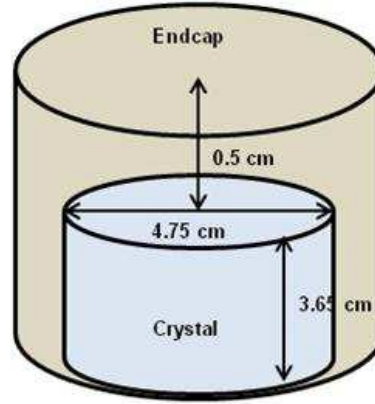


Figure 2.3: Detector dimensions

2.3 HPGe Calibration

A spectrum was obtained using one of the Eu-152 standard sources allowing for energy calibration following G2K software specifications (Fig. 2.4) (Canberra, 2009, p.70).

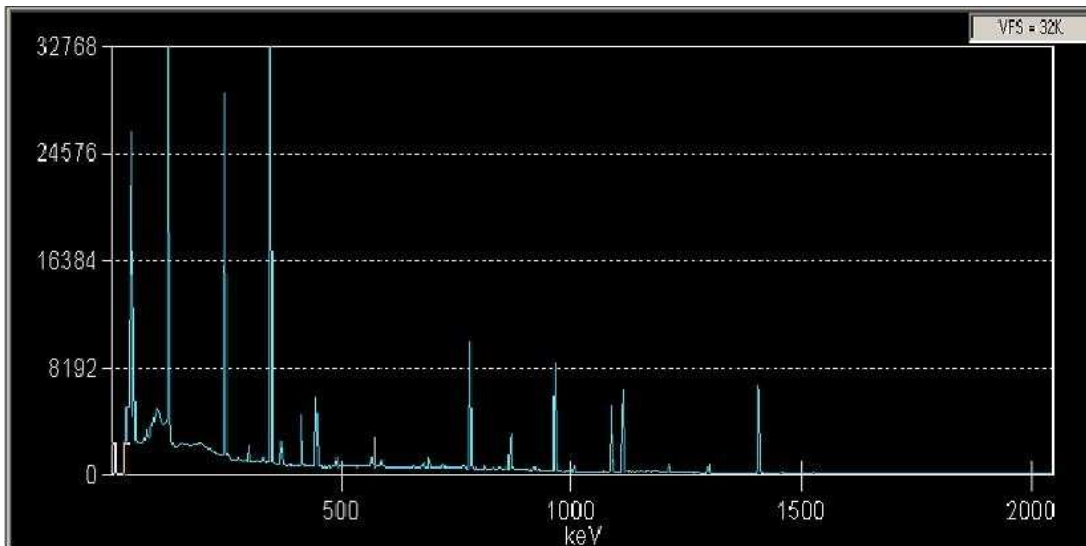


Figure 2.4: Eu-152 spectrum

Eu-152 exhibits coincidence summing and therefore a cascade correction is necessary. Single nuclide spectra were obtained for Cd-109, Cs-137, and Mn-54. These spectra were utilized to perform a peak-to-total calibration with the G2K software (Canberra, 2009, p. 249). Multi-source calibration allows the software to perform a cascade correction, thereby improving detector efficiency and decreasing activity uncertainty.

Table 2.3: Efficiency calibration configurations

Position	Attenuator		Sample Geometry		
A	Corner	1	Air	\$	Small type A shipping can
B	Well	2	Water Marinelli	%	Sealed disk source
C	Middle Shelf	3	Lead	&	Bag
D	Top Shelf				
E	0.5 cm spacer				
F	5.5 cm spacer				
G	No spacer				

Cascade correction was used in conjunction with efficiency calibration curves for multiple geometries. Each position, attenuator, and sample geometry were given a reference for identification purposes. Table 2.3 lists the geometry reference identification codes. A small type A shipping can (Fig. A.4) placed into the well with a water Marinelli attenuator would be identified as \$B2.

$$\epsilon_i = \frac{\text{dps } Y_i}{\text{cps}} \quad (2.3)$$

where ϵ_i = efficiency

dps = decay corrected activity (Bq)

Y_i = branching ratio

cps = total counts per time interval.

For each configuration, a Eu-152 standard was utilized to obtain a spectrum for 5400 seconds. The net peak area for each of the 10 main photopeaks of Eu-152 was recorded for each configuration. Using the net peak area and the decay corrected standard activity, an efficiency value for each of the 10 photopeaks in each configuration was calculated using equation 2.3. The empirically derived photopeak efficiencies were used to perform an efficiency calibration following G2K software specifications (Canberra, 2009, p.87).

2.4 Detector Dead Time

Facility specifications for detector dead time are equal to or less than 10%. Determination of the importance of detector dead time was performed using a sample of bolts removed from the reactor room. The sample of bolts was counted sequentially using three effective geometry ID codes from Table 2.3: \$B1 (small shipping can in lead cave well with air attenuator), \$A1 (small shipping can on corner of lead shielding with air attenuator), and \$E1 (small shipping can on 0.5 cm spacer with air attenuator). The detector dead time in these three configurations were respectively: 1.11%, 15.17%, and 86.08% respectively.

2.5 Attenuators

The majority of samples at this facility are neutron activation products, therefore the presence of a wide range of gamma energies during spectroscopy can be expected. Samples are typically high activity ranging from μCi to mCi (milliCurie) levels resulting in detector dead time above the facility accepted 10%. Increasing distance can reduce detector dead time, however the amount of distance required is not always feasible. The detector room is located directly off of a main corridor and shares walls with offices and other laboratories. Radiation levels must be kept as low as reasonably achievable (ALARA) to maintain safety for all workers in the building. Therefore, an attenuator system was developed and tested. The attenuator system allows the sample container to be placed at a reasonable, yet still shielded distance from the detector while reducing detector dead time.

The two attenuators tested were 1) a 9.96 mm (0.38 in.) lead brick encased in duct tape (Fig. A.5) placed in the well above the detector and 2) a standard Marinelli beaker containing 1 L (liter) of water (Fig. A.6) placed directly on the detector. Both attenuators were tested for accuracy. Accuracy testing was performed by placing the

lead attenuator in the well while obtaining sample data. The procedure was repeated by placing the 1 L water Marinelli over the detector during sample acquisition. Next, the small type A shipping can containing Eu-152 standard was placed in position C (middle shelf of lead cave) and a spectrum obtained using both lead and water attenuators in combination. The experimental attenuation coefficient values were compared to theoretical values from Hubbell and Seltzer (1996).

2.6 Current Method of Activity Determination

The method of activity determination utilized by reactor staff prior to this study involved multiple steps. First, a hand-held ion chamber (Fluke Biomedical Model 451B) was placed at a distance of one foot (30 cm) from a small type A shipping can and a value of exposure rate was obtained in units of mR h^{-1} per equation 2.4 (Radiological Health Handbook, 1970, p.205). This rule of thumb is quoted by Radiological Health Handbook to be within 20% for point source gamma emitters with energies between 0.07 and 4 MeV at 1 foot. For calculation purposes, the value of En was assumed to be 1 for all samples and equation 2.4 was solved for the value of C .

$$R h^{-1} \approx 6 C E n \quad (2.4)$$

where $R h^{-1}$ = exposure rate

C = activity (Ci)

E = photon energy (MeV)

n = fraction of transformation resulting in photon energy E

Next, the same type A shipping can was placed near the HPGe in a position resulting in an acceptable amount of detector dead time, which is less than 10% for this facility. No efficiency calibration was loaded into the G2K software. A nuclide identification sequence was performed with the G2K software, which provided a weighted mean activity in μCi for each nuclide identified. The total sample activity

calculated with equation 2.4 was divided into individual nuclide activities per the nuclide activity ratio provided by the G2K software.

2.7 Proposed Method of Activity Determination

Following energy and efficiency calibration procedures of the HPGe, the weighted mean activity from the G2K software can be utilized for activity determination without the use of a hand-held ion chamber or equation 2.4. The proposed method for nuclide identification and activity determination was to dispense with the hand-held ion chamber for activity determination and rely solely on the activity values provided by the G2K software. Calculation of the weighted mean activity in the G2K software requires multiple internal operations, which utilize equations 2.5, 2.6, and 2.7.

$$A_i = \frac{S}{V\epsilon Y T_l U K A} \quad (2.5)$$

where S = net peak area

V = sample volume/mass

ϵ = attenuation corrected efficiency

Y = branching ratio

T_l = live time (sec)

U = conversion factor from Bq to Ci

K = correction factor for decay during counting [Eq. 2.6]

A = decay corrected activity (Bq).

$$K = \frac{T_{1/2}}{\ln(2)t_c} \left(1 - e^{-\frac{\ln(2)t_c}{T_{1/2}}}\right) \quad (2.6)$$

where $T_{1/2}$ = radionuclide half life (t)

t_c = elapsed real clock time (t).

$$C_{Av} = \frac{\sum_{i=1}^N \frac{C_i}{\sigma_{Ci}^2}}{\sum_{i=1}^N \frac{1}{\sigma_{Ci}^2}} \quad (2.7)$$

where C_{Av} = decay corrected weighted average activity

N = number of nuclide energies identified

C_i = decay corrected activity of the i^{th} energy

σ_{Ci} = standard deviation of C_i .

CHAPTER 3

Results

3.1 Efficiency Curves

HPGe calibration required the development of multiple sets of efficiency curves. The R-squared value for each curve was used to determine the accuracy of curve fit. All R-squared values were greater than 0.94.

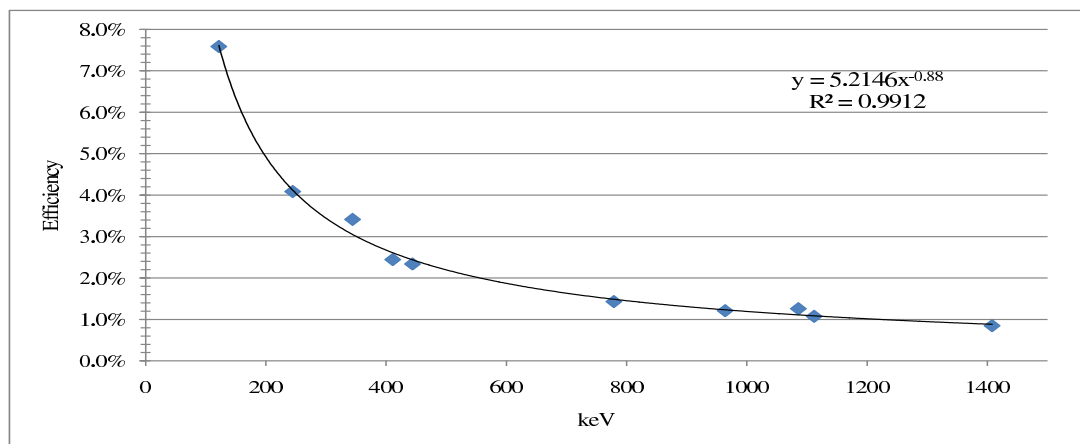


Figure 3.1: Efficiency curve for Eu-152 standard centered on 0.5 cm spacer.

3.2 Dead Time Analysis

A sample of bolts from the reactor room was counted in three separate geometries resulting in three detector dead times. The theoretical keV for the identified radionuclides was graphed against the difference between theoretical keV and experimental

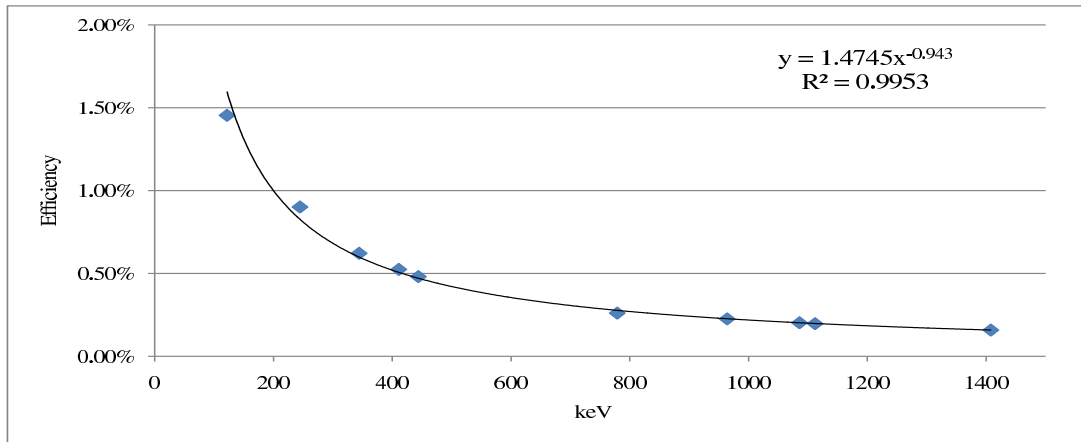


Figure 3.2: Efficiency curve for Eu-152 standard centered on 5.5 cm spacer

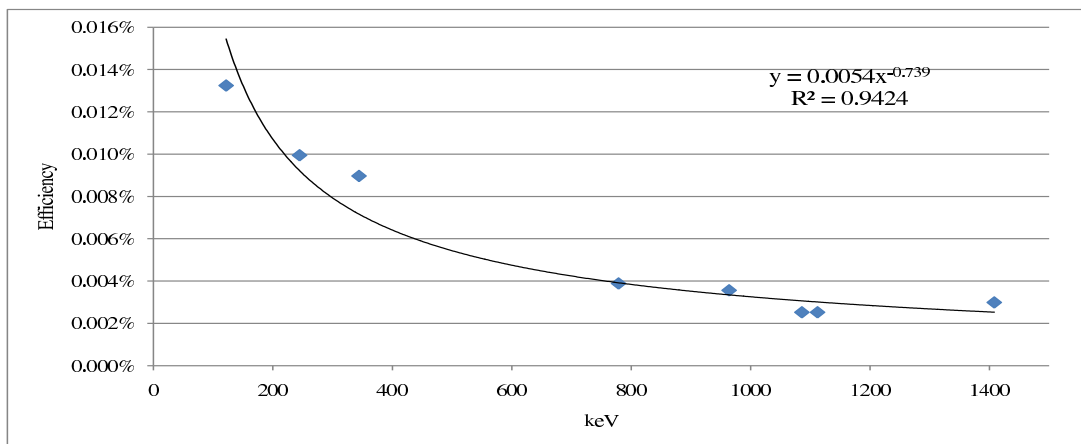


Figure 3.3: Efficiency curve for Eu-152 standard in position %A1

keV at each detector dead time (Fig. 3.4).

The dashed line in figure 3.4 at 1 on the y-axis represents the keV tolerance range typically used by the G2K software. The tolerance range is based on identified photopeaks which are within one keV of theoretically expected nuclide photopeak values. The dashed line at 1.5 on the y-axis represents a keV tolerance range that is just slightly wider than the standard used by the G2K software.

Using the standard 1 keV tolerance range and 1.1% dead time, fifteen photopeaks were identified. Increasing the dead time to 15.17% reduced the identification to fourteen photopeaks. A further increase in the dead time to 86.08% further reduced identification to two photopeaks.

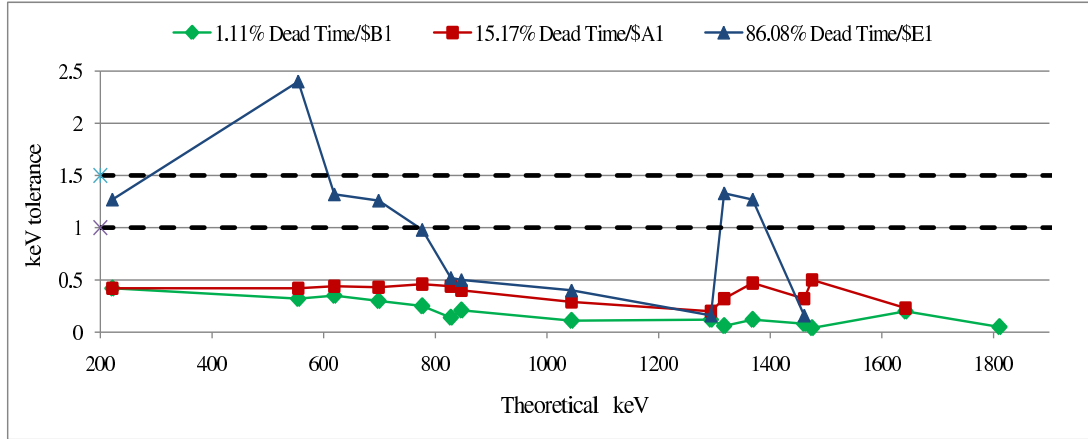


Figure 3.4: Comparison of identified peaks at various dead-times

Repeating this procedure using a wider 1.5 keV tolerance allowed for identification of all fifteen photopeaks at 1.11% and 15.17%. A total of eleven photopeaks were identified at 86.08% dead time.

3.3 Attenuation Coefficients

Accuracy testing of the lead brick and water Marinelli attenuators was performed. A graph of theoretical attenuation coefficient compared with experimental total attenuation coefficient for each attenuator was created (Figs. 3.5, 3.6).

All experimental values were within one standard deviation of the theoretical value. Variations from theoretical values are likely due to scattering within the detector shielding.

3.4 Comparison Using Various Attenuators

Different attenuator materials have varying effects on the shape of the efficiency curve for Eu-152 standards. The water attenuator causes a mostly flat response across the Eu-152 spectrum while a lead attenuator causes a large decrease in efficiency below 600-800 keV. A graph was created using a Eu-152 standard on the middle shelf of the lead cave. A curve for air attenuator only (%C1), water attenuator only (%C2), and

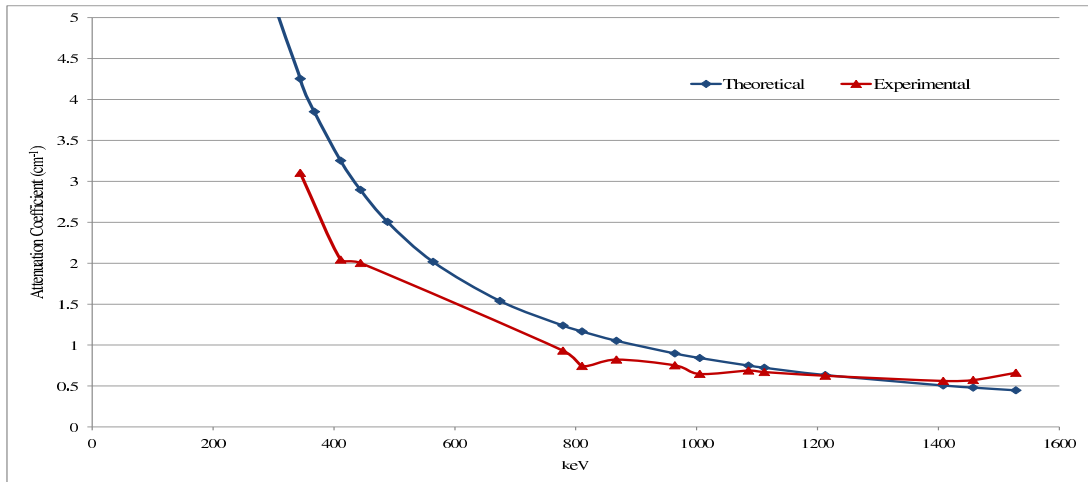


Figure 3.5: Comparison of lead attenuation coefficients

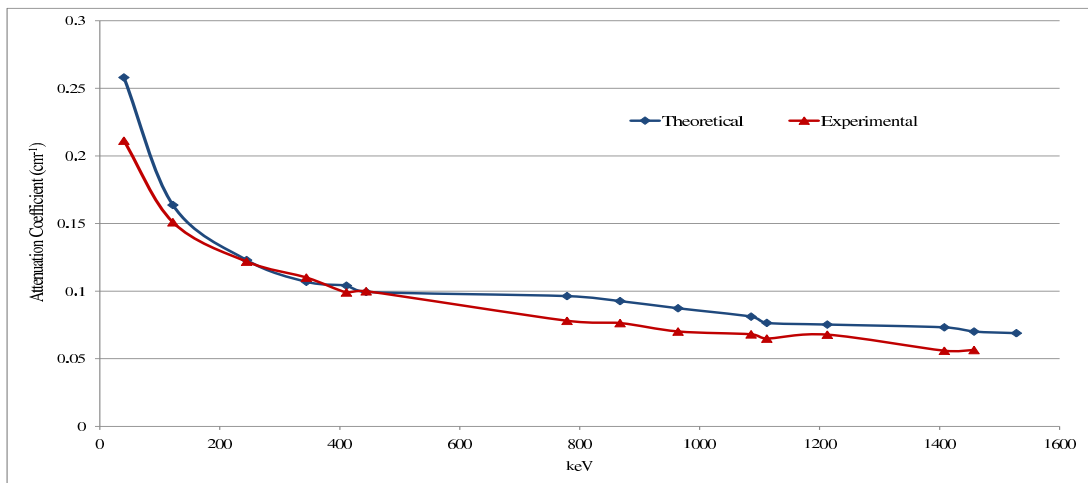


Figure 3.6: Comparison of water attenuation coefficients

water and lead attenuator combo (%C23) were graphed (Fig. 3.7).

A second graph (Fig. 3.8) was created using the same standard, position and attenuators, however for this graph the Eu-152 was placed inside of a small type A shipping can. The efficiency curve shape for each attenuator are relatively consistent, however the overall efficiency is reduced due to shielding from the shipping can.

3.5 Method Comparison

Data from multiple radioactive material shipments of the USGS (U.S. Geological Survey) neutron activation samples were obtained (Appendix D.1). The activity

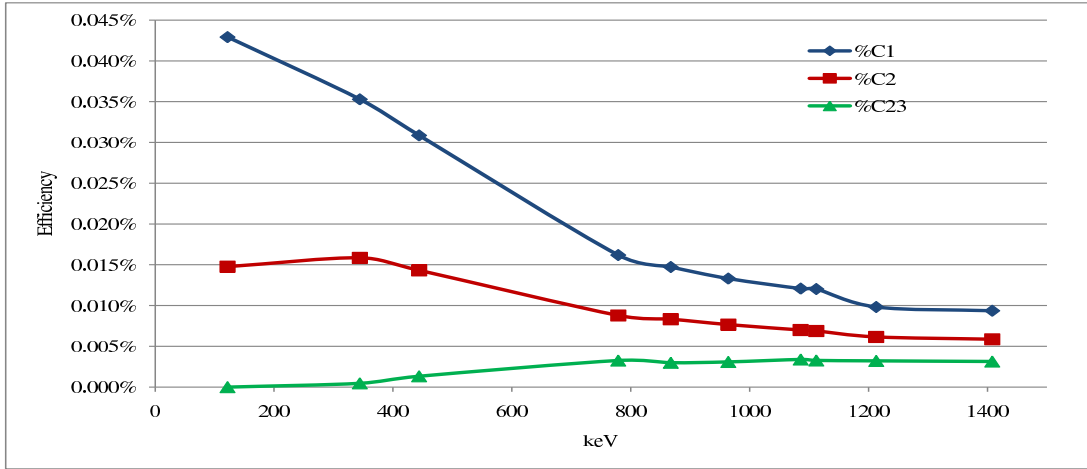


Figure 3.7: Efficiency curves for Eu-152 standard.

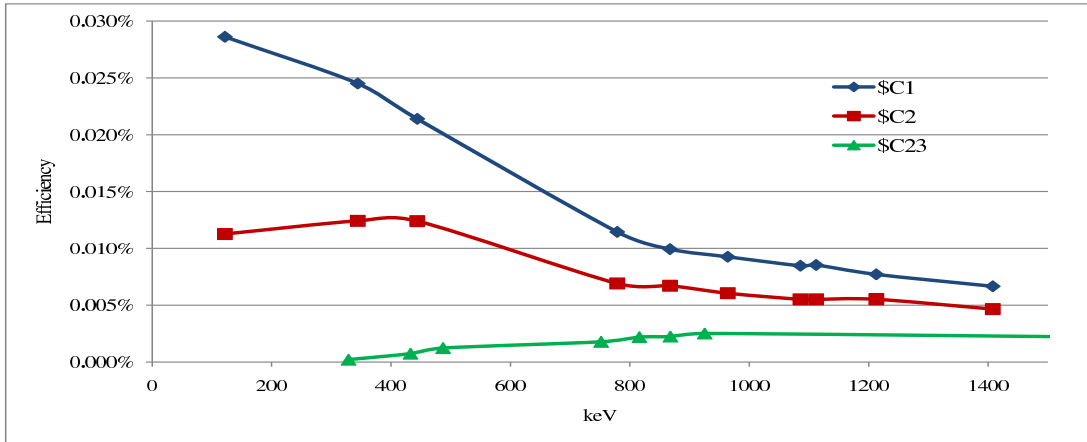


Figure 3.8: Efficiency curves for Eu-152 standard in small type A shipping can.

per nuclide of each shipment was determined using both the proposed new method consisting of data from the G2K software as well as the original method consisting of a thumb rule given in equation 2.4 with an assumption that $E_n = 1$.

Data from shipments with and without Na-24 were graphed separately to investigate for consistency in analysis data. The data from the shipments with Na-24 follow two distinct trends (Fig. 3.9).

This data indicates that the points along the 1:1 line have G2K to equation 2.4 ratios less than 1.4. The shipment data with ratios greater than 1.4 fall along the dashed line. To investigate this discrepancy, a log-log graph was plotted for each isotope individually with the G2K to equation 2.4 ratio on the y-axis and the G2K activity

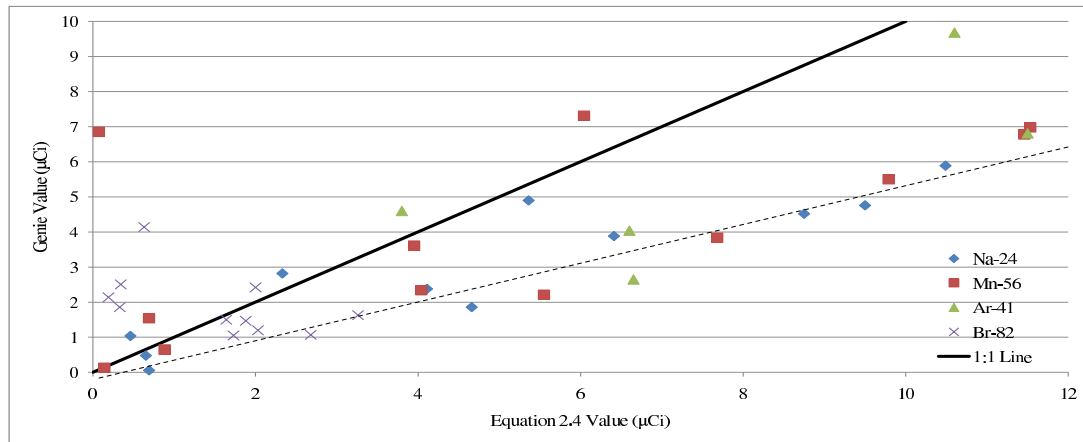


Figure 3.9: Shipments containing Na-24 ($E n=1$ assumption)

on the x-axis. Note that there are some data points visible on Fig. 3.10 that were not included on Fig. 3.9. Each data set was fitted with a linear trendline. Of these four graphs, only the graph of Na-24 indicated any linearity, with a resultant R-squared value of 0.75 (Fig. 3.10). This represents a strong correlation that the presence of Na-24 in the sample is the cause of the differentiation in the data sets.

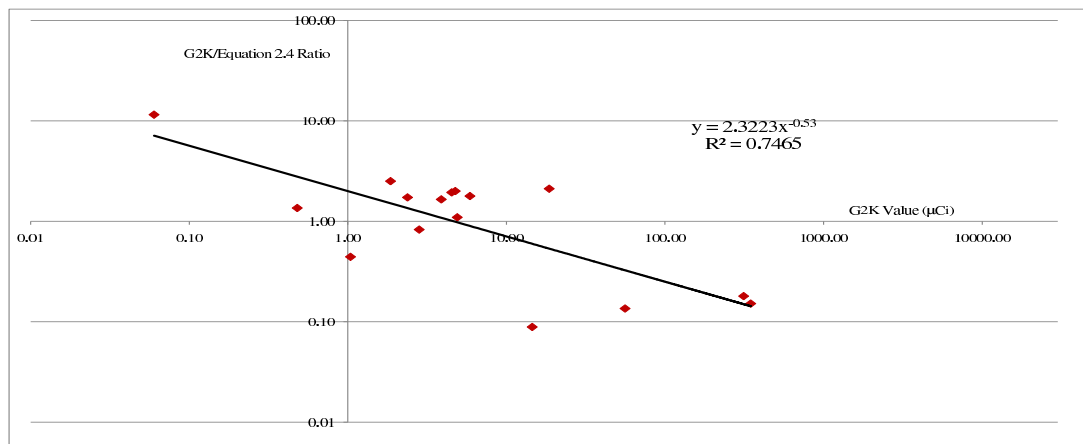


Figure 3.10: Log-log graph of Na-24 effect on G2K value

The graph of the shipment data without Na-24 indicates that very few data points actually fall near the 1:1 line (Fig. 3.11). The cause of the randomness of this data is not readily apparent.

The validity of equation 2.4 is called into question based on this data. Thus, further analysis was performed. A full calculation of each shipment using equation

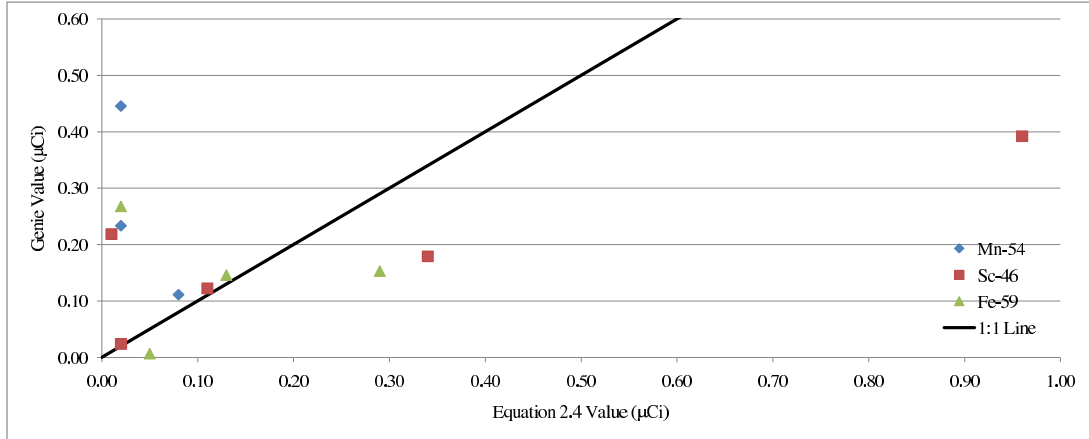


Figure 3.11: Shipments not containing Na-24 ($En=1$ assumption)

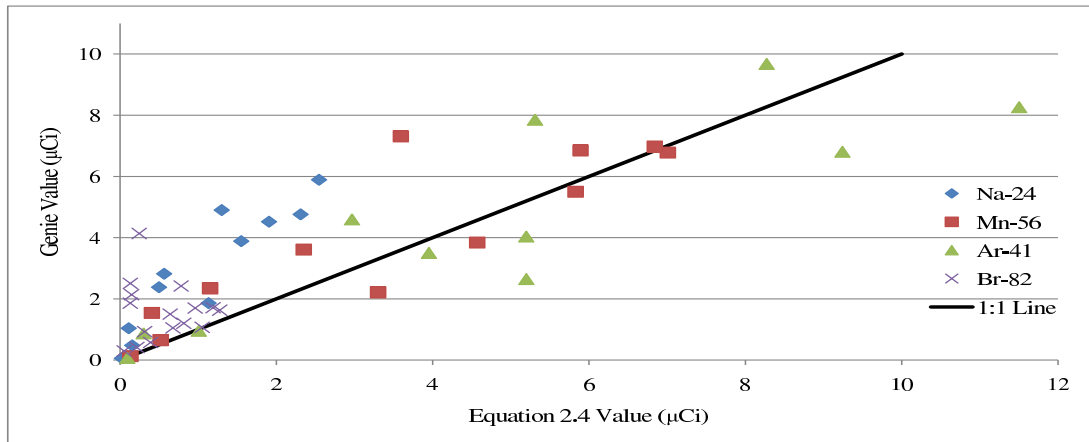


Figure 3.12: Shipments containing Na-24 (no En assumption)

2.4 was performed using actual nuclide energies and photon yields for each nuclide, rather than assuming $En=1$. This activity value was graphed against the activity value provided by the G2K software (Figs. 3.12, 3.13). The full calculation of equation 2.4 solves the issue of the two distinct data sets seen when using the $En=1$ assumption with shipments containing Na-24. Alternatively, performing the full calculation for shipments not containing Na-24 does little to improve the data.

3.6 Further Testing of Equation 2.4 Validity

The GSTR was utilized for an experiment where a 0.0123 g (gram) sample of NaOH was irradiated for 5 minutes in a thermal neutron flux of 7.5×10^{11} neutrons per

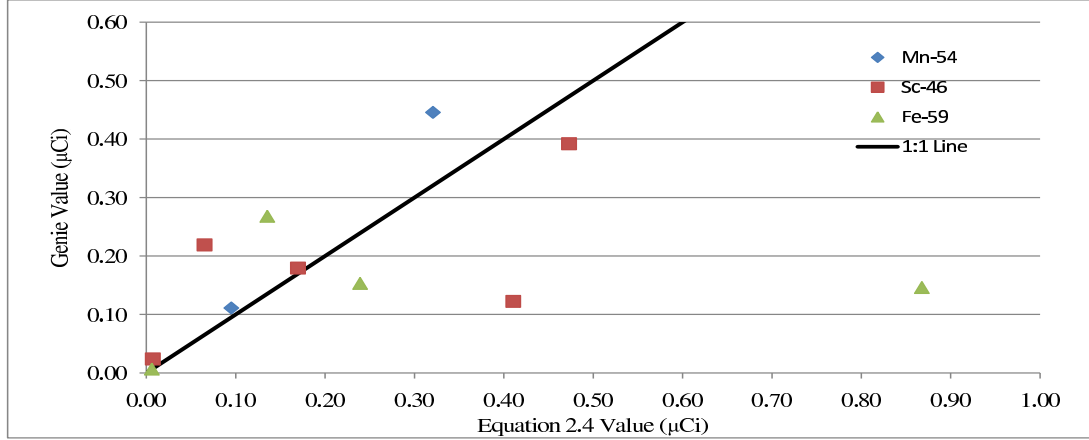


Figure 3.13: Shipments not containing Na-24 (no En assumption)

Table 3.1: NaOH experiment

Equation 2.4 with $En = 1$		20 μCi	
Equation 2.4 with $En = 4.12$		4.85 μCi	
Activity of Na-24 (μCi)	Position	Attenuator	Geometry
4.07	5.5 cm spacer	Air	Disk source
4.85	Middle shelf lead cave	Air	Disk source
5.64	Corner	Air	Small shipping can
4.70	Well	Water Marinelli	Small shipping can
5.07	Well	Air	Disk source
3.81	5.5 cm spacer	Air	Disk source

square centimeter-second to produce a sample containing predominantly Na-24. The sample was evaluated using the hand-held detector as well as in multiple geometries with the G2K software (Table 3.1).

The activity calculated using equation 2.4 with an assumed En value of one is four times greater than the activity calculated using an En value of 4.12 (Eq. 3.1).

$$En_{(\text{Na-24})} = (1.369 \text{ MeV} \times 1.00) + (2.754 \text{ MeV} \times 0.999) = 4.12 \quad (3.1)$$

Eu-152 standards were also utilized for equation 2.4 verification (Tables 3.2, 3.3). This data indicates the activity from equation 2.4 and $En = 1$ is 3 orders of magnitude different than the decay corrected activity of the Eu-152 standard. The values

obtained using the G2K software are mostly within one standard deviation of the decay corrected activity.

Table 3.2: Equation 2.4 values obtained for Eu-152 standard

Geometry	Background	Meter value	Eq. 2.4	Eu-152 activity
In small shipping can	9	22	2167	2.28
Disk source	9	23	2333	2.28
In waste bag	9	21	2000	2.28

Table 3.3: Genie values obtained using Eu-152 standard

Geometry	Attenuator	Position	G2K	Eu-152 activity
Waste bag	Air	0.5 cm spacer	1.64 ± 0.38	2.28
Small shipping can	Water Marinelli	A	2.36 ± 0.54	2.28
Small shipping can	Water Marinelli and lead brick	Middle shelf lead cave	2.40 ± 0.93	2.28

Background and meter value have units of mR h^{-1} .

Equation 2.4 and decay corrected activity have units of μCi .

CHAPTER 4

Conclusion

4.1 Attenuators and Efficiency

Attenuator accuracy testing indicates the experimental values for the attenuation coefficients utilized for this study are within one standard deviation of the theoretical values. Additionally, efficiency curves were generated for multiple geometries both with and without the presence of attenuators. These efficiency curves were found to have good fit in both cases. Sampling has proven that these efficiency curves are valid.

For every container geometry and position, there exists an efficiency calibration, which the reactor staff have been trained to utilize.

4.2 Detector Dead Time

Current facility specifications state the detector dead time should be 10% or less for nuclide identification analysis. 10% or less detector dead time is achievable through the use of the developed lead cave resulting in a geometric reduction in photon flux.

Higher detector dead times and a wider keV tolerance are also very reasonable nuclide identification options. This configuration was proven to be comparable to identification at low detector dead time and more narrow keV tolerance.

4.3 Method Comparison

The use of the assumption of En equal to one for equation 2.4 was found to be a very inaccurate method of activity determination. This assumption can lead to activity values several orders of magnitude higher than other methods. The use of the energy and efficiency calibrated G2K software as a stand-alone method was more accurate and required less steps.

The use of equation 2.4 using full nuclide energy and yield information for the shipments containing Na-24 was fairly accurate and could be used in conjunction with the G2K software for validation purposes. However, this same calculation for shipments not containing Na-24 was not found to be as accurate. The reason for this inaccuracy was not determined.

4.4 Further Studies

Further investigation into the inaccuracy of equation 2.4 for shipments not containing Na-24 would be appropriate. The data obtained during this study seemed to indicate that Cr-51 could be the contributing factor, however a sufficient amount of data to confirm this hypothesis was not available.

Overall shipment activity determination using equation 2.4 for shipments containing Na-24 was fairly accurate. However, discrepancies with individual nuclide activity determination was demonstrated. This could be due to the large Compton edge associated with the Na-24 spectrum. Further investigation of this effect could possibly be performed utilizing a sample with Na-24 in combination with another activation product with a half-life of approximately 60 hours. Gamma spectroscopy of a test sample could be performed as soon as possible after irradiation and then at regular intervals until the Na-24 has decayed below distinguishable levels to ascertain the impact of Na-24.

Bibliography

- Canberra GenieTM 2000 V3.1 Operations Manual. Canberra, Meriden, CT; 2006.
- Canberra glossery. Available at: <http://www.canberra.com/literature/930.asp>. Accessed 1 September 2010.
- Cember H and Johnson TE. Introduction to Health Physics, 4th ed; 2009.
- Debertin K and Schötzig U. Coincidence Summing Corrections in Ge(Li)-Spectrometry at Low Source-To-Detector Distances. Nuclear Instruments and Methods 158:471-477; 1979.
- Electronic Code of Federal Regulations. Title 49 - Transportation, Part 172-173. Available at: http://ecfr.gpoaccess.gov/cgi/t/text/text-idx?c=ecfr&tpl=/ecfrbrowse/Title49/49cfrv2_02.tpl. Accessed 1 September 2010.
- Gollnick DA. Basic Radiation Protection Technology, 4th ed; 2004.
- Hubbell JH, Seltzer SM. Tables of X-ray mass attenuation coefficients and mass energy-absorption coefficients from 1 keV to 20 MeV for elements $Z = 1$ to 92 and 48 additional substances of dosimetric interest. Ionizing Radiation Division, Physics Laboratory, NIST. Available at: <http://www.nist.gov/pml/data/xraycoef/index.cfm>. Accessed 12 July 2010.
- Knoll GF. Radiation Detection and Measurement, 3rd ed; 2000.
- Martin JE. Physics for Radiation Protection, 2nd ed; 2006.

Martin R, Knauer J, and Balo P. Production, distribution, and applications of californium-252 neutron sources. Technical Paper, IRRMA 4th Topical Meeting on Industrial Radiation. Raleigh, NC; 1999.

Serway RA and Jewett JW Jr. Physics for Scientists and Engineers, 6th ed; 2004.

Shleien B, Lester J, Slaback A, and Birky B. Handbook of Health Physics and Radiological Health, 3rd ed; 1998.

U.S. Department of Health, Education and Welfare. Radiological Health Handbook; 1970.

United States Geological Survey, Central Region Geology. GSTR services. Denver, CO; 2005. Available at: <http://geology.cr.usgs.gov/facilities/gstr/>. Accessed 1 September 2010.

Appendix A: Photos



Figure A.1: Detector inside shielding

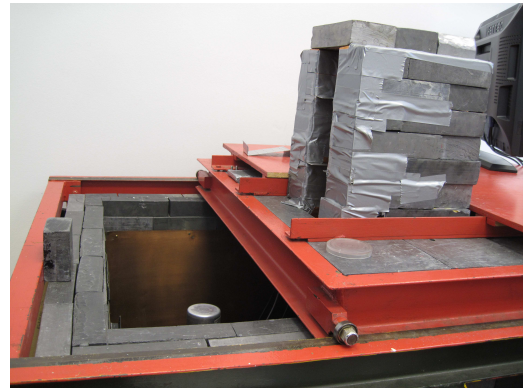


Figure A.2: Shielding with lid open



Figure A.3: Eu-152 sealed sources

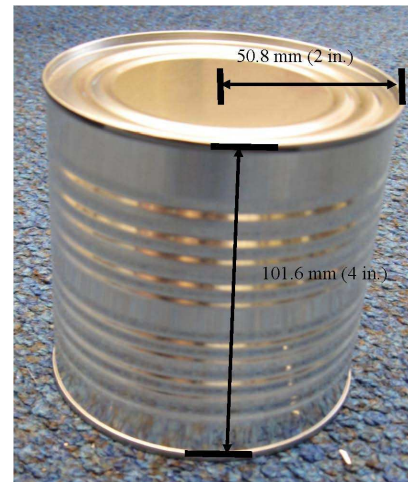


Figure A.4: Small type A shipping can

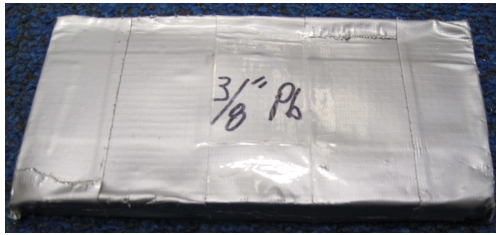


Figure A.5: Lead attenuator

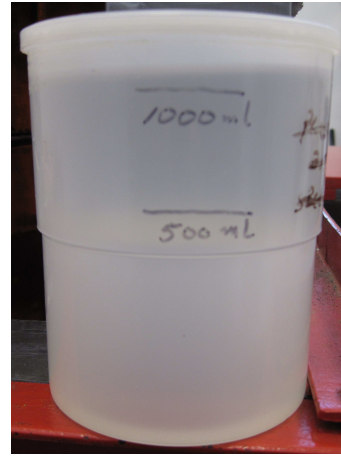


Figure A.6: Water Marinelli attenuator

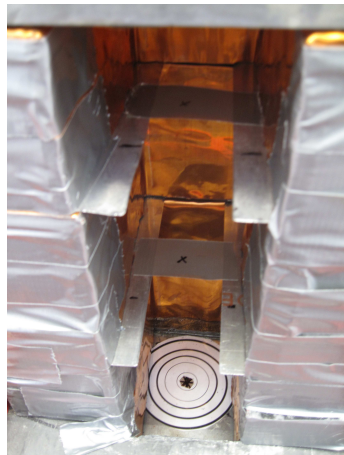


Figure A.7: Inner view of lead cave



Figure A.8: Position \$A2

Appendix B: Derivation of Equation 2.4

$$\dot{X} \text{ (Exposure Rate)} = \frac{\mathcal{F} \frac{\text{photons}}{\text{dis}} \times E \frac{\text{MeV}}{\text{photon}} \times (1.6 \times 10^{-13}) \frac{\text{J}}{\text{MeV}} \times \frac{\mu_a}{\text{cm}} \times (1 \times 10^6) \frac{\text{dps}}{\text{MBq}}}{\rho \frac{\text{kg}}{\text{cm}^3} \times 34 \frac{\text{J/kg}}{\text{C/kg}} \times 4\pi (\text{m})^2}$$

$$= \frac{\mathcal{F} \frac{\text{photons}}{\text{dis}} \times E \frac{\text{MeV}}{\text{photon}} \times (1.6 \times 10^{-13}) \frac{\text{J}}{\text{MeV}} \times \frac{0.00107}{\text{ft}} \times 1 \frac{\text{dps}}{\text{Bq}} \times (3.7 \times 10^{10}) \frac{\text{Bq}}{\text{Ci}} \times 3600 \frac{\text{s}}{\text{h}}}{\frac{1.293 \text{ kg}}{35.3 \text{ ft}^3} \times 34 \frac{\text{J/kg}}{\text{C/kg}} \times \frac{1 \text{ C/kg}}{3881 \text{ R}} \times 4\pi (\text{m})^2 \left(\frac{\text{ft}^2}{0.0929 \text{ m}^2}\right)}$$

$$= \frac{\mathcal{F} \frac{\text{photons}}{\text{dis}} \times E \frac{\text{MeV}}{\text{photon}} \times (2.3 \times 10^{-2}) \frac{\text{J dis}}{\text{ft Ci h MeV}}}{10.76 \text{ ft}^2 \times 0.037 \frac{\text{kg}}{\text{ft}^3} \times 0.0088 \frac{\text{J/kg}}{\text{R}}}$$

$$\frac{R}{h} = \mathcal{F} \frac{\text{photons}}{\text{dis}} \times E \frac{\text{MeV}}{\text{photon}} \times C(\text{Ci}) \times 6.586 \frac{\text{dis}}{\text{MeV Ci}}$$

$$\frac{R}{h} = 6 E C n$$

The value for μ_a can be found in Figure 5.20 of Cember and Johnson.

$$\text{At 1 MeV, } \mu_a \approx \frac{3.5 \times 10^{-5}}{\text{cm}} = \frac{0.00107}{\text{ft}}$$

Appendix C: Background

Germanium Detectors

Electrical conductors are materials in which some of the electrons are unbound and can move relatively freely through the material. Electrical insulators are materials in which all electrons are bound and are unable to move freely. A semiconductor is a third class of materials with properties between those of conductors and insulators (Serway and Jewett, 2004). Germanium has been identified as having good semiconductor properties.

Germanium consists of four valence electrons which form a lattice of atoms joined together by covalent bonds (Cember et al., 2009). Absorption of energy into the lattice disrupts the covalent bonds, which eject a free electron. A resultant hole in the lattice in the space formerly occupied by the electron is formed. This cause and effect relationship indicates that the number of free electrons must exactly equal the number of lattice holes (Knoll, 2000). Material impurities allow for two types of conductors to exist: *n*-type and *p*-type. *n* represents the concentration of free electrons and *p* represents the concentration of holes in the crystal lattice.

The sensitive volume of the germanium crystal is in the presence of a constant electric field. The process of creating an electron-hole pair creates a current, which are collected at the the boundary of the sensitive volume by diode. The current from the diode is amplified and sent to a MCA (multi-channel analyzer) employing gamma spectroscopy analysis software, such as the G2K software.

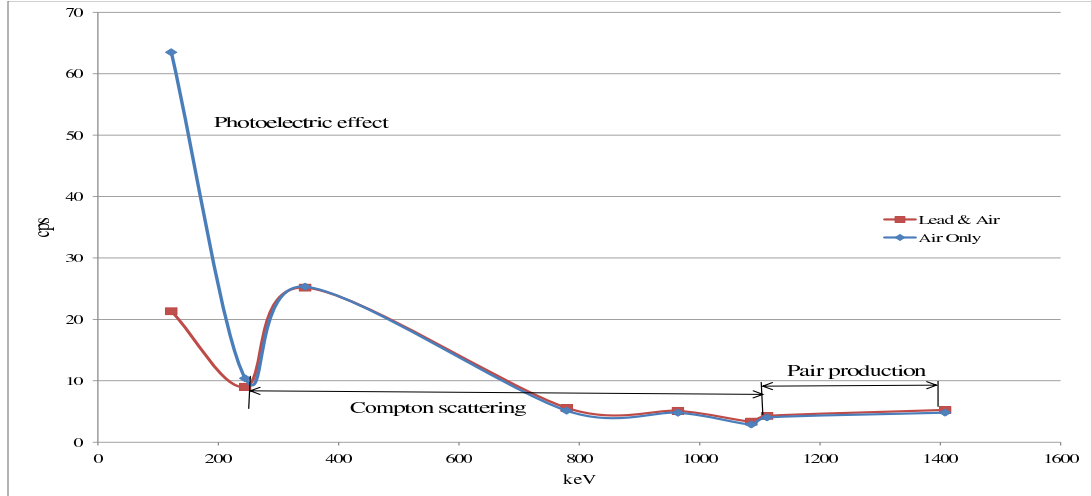


Figure C.1: Graph of gamma-ray interactions

Gamma-Ray Spectra

Gamma-rays are emitted monoenergetically following radioactive transformations within the nuclei of excited atoms (Cember et al., 2009). The type of radioactive transformation that occurs is dependent on the gamma-ray energy (Fig. C.1). For gamma-ray energies less than 500 keV, the photoelectric effect (Fig. C.2) is the most likely method of interaction with materials (Martin, 2006). Photoelectric effect (PE) is an interaction between a photon and a tightly bound electron. The probability of PE interaction increases with binding energy. When photons collide with a bound orbital electron, they are ejected from the atom. The electron is ejected with an energy equal to that of the incoming photon minus the binding energy of the electron. The greatest binding energy is typically found in K shell electrons. The ejected photoelectron deposits its energy in the absorbing medium through excitation and ionization. This energy deposition is detected, thus resulting in a photopeak corresponding to the energy of the incident gamma rays (Knoll, 2000).

Compton scattering occurs when a gamma-ray interacts with a free or weakly bound electron (Fig. C.3). The gamma-ray photon strikes an atom and is deflected at an angle θ with respect to its incoming direction (Knoll, 2000). Additionally, an

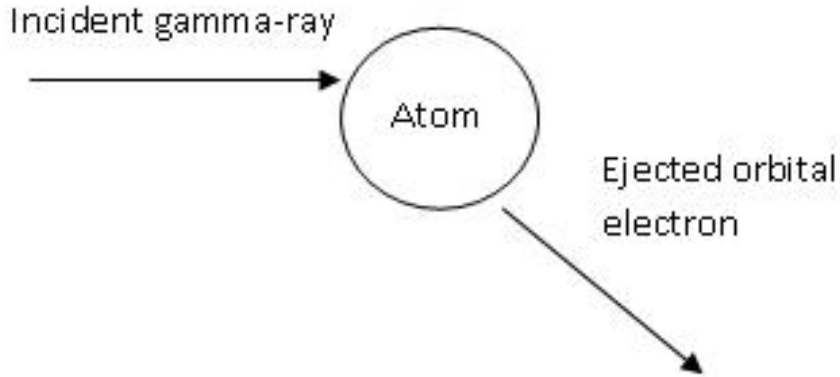


Figure C.2: Schematic of photoelectric effect

ejected electron from the atom travels away from the interaction site with an energy that is equal to that of the incoming gamma-ray minus the energy of the scattered gamma-ray (Eq. C.1).

$$E_e = E_\gamma - E' \quad (\text{C.1})$$

where E_e represents energy of the scattered electron

E_γ represents energy of the incident gamma-ray

E' represents energy of the scattered gamma-ray.

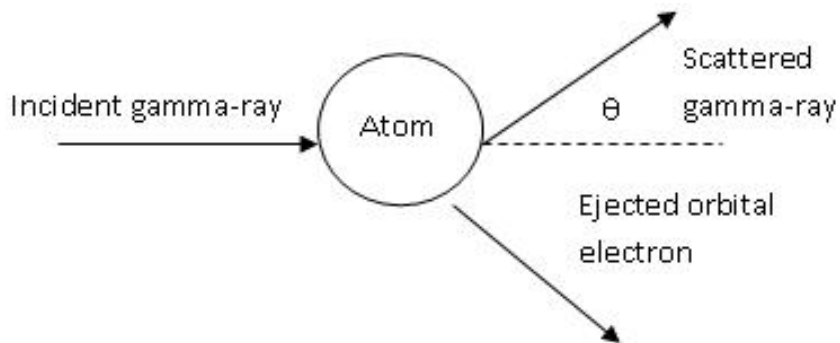


Figure C.3: Schematic of Compton scattering

Multiple Compton scattering interactions can take place within the detector simultaneously. A continuum of energies for the ejected electron is produced, ranging

from 0 up to a maximum defined by equation C.2. The value of θ can range from 0 to 180 degrees. The value of θ and the value of E_e are directly proportional. The ideal gamma-ray spectra would have narrow, tall photopeaks to indicate specific energies. Therefore, the signal from a germanium detector is passed through anticoincidence circuitry to minimize the Compton continuum (Knoll, 2000).

$$E_e = hv \frac{\left(\frac{hv}{m_0c^2}\right)(1 - \cos \theta)}{1 + \left(\frac{hv}{m_0c^2}\right)(1 - \cos \theta)} \quad (\text{C.2})$$

where E_e represents the energy of the scattered electron

h represents Planck's constant

v represents the frequency of the incoming gamma-ray photon

m_0c^2 represents the rest mass of an electron (0.511 MeV)

θ represents the angle of gamma-ray scattering.

Gamma-ray photons with energies greater than approximately 1.022 MeV typically interact via pair production (PP) (Fig. C.4). Two electrons are formed during pair production. PP only occurs above 1.022 MeV due to the need for energy equivalence of the rest mass of two electrons (0.511 MeV). A gamma-ray photon that encounters the electromagnetic field of a nucleus can spontaneously disappear. The gamma-ray energy is converted into a positron and electron pair, which appear simultaneously. The kinetic energy of the pair is reduced by absorption in the detector. The positron will combine with another electron, releasing two gamma-rays, each with energy equivalent to the rest mass of an electron. These two gamma-rays are known as annihilation gammas. Three scenarios are possible once annihilation has occurred. Both annihilation gamma-rays can escape from the detector resulting in a double-escape peak, which has an energy 1.022 MeV less than the full-energy peak. Only one of the annihilation gamma-rays escaping the detector results in a single-escape peak with an energy 0.511 MeV less than the full-energy peak. Both

annihilation gamma-rays captured by the detector results in their energy contributing to the full-energy peak of the gamma spectra.

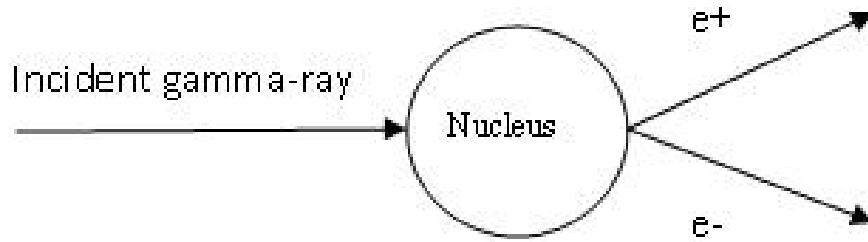


Figure C.4: Schematic of pair production

Appendix D: USGS Shipment Data

Data for 22 shipments was provided by the staff of the GSTR staff.

G2K and equation 2.4 values have units of μCi .

Table D.1: USGS shipment data

ID	Isotope	G2K	Eq. 2.4	Eq. 2.4/G2K	Position	Attenuator	Geometry
94	Na-24	2.38	4.11	1.73	5.5 cm spacer	Air	Small shipping can
94	Cl-38	3.60	6.23	1.73	5.5 cm spacer	Air	Small shipping can
94	Ar-41	7.86	13.58	1.73	5.5 cm spacer	Air	Small shipping can
94	K-42	0.14	0.23	1.64	5.5 cm spacer	Air	Small shipping can
94	Mn-56	2.34	4.04	1.73	5.5 cm spacer	Air	Small shipping can
94	Br-82	0.93	1.61	1.73	5.5 cm spacer	Air	Small shipping can
94	Zr-97	0.01	0.02	2.00	5.5 cm spacer	Air	Small shipping can
94	Ba-139	0.11	0.18	1.64	5.5 cm spacer	Air	Small shipping can
	Total	17.35	30.00	1.73			
89	Na-24	0.48	0.65	1.35	5.5 cm spacer	Air	Small shipping can
89	Cl-38	1.15	1.55	1.35	5.5 cm spacer	Air	Small shipping can
89	K-40	0.04	0.05	1.25	5.5 cm spacer	Air	Small shipping can

continued on next page

continued from previous page

ID	Isotope	G2K	Eq. 2.4	Eq. 2.4/G2K	Position	Attenuator	Geometry
89	Ar-41	0.96	1.29	1.34	5.5 cm spacer	Air	Small shipping can
89	Mn-54	0.02	0.02	1.00	5.5 cm spacer	Air	Small shipping can
89	Mn-56	0.65	0.88	1.35	5.5 cm spacer	Air	Small shipping can
89	Br-82	0.41	0.55	1.34	5.5 cm spacer	Air	Small shipping can
89	W-187	0.02	0.02	1.00	5.5 cm spacer	Air	Small shipping can
	Total	3.73	5.01	1.34			
88	Na-24	0.06	0.69	11.50	5.5 cm spacer	Air	Small shipping can
88	Ar-41	0.07	0.08	1.14	5.5 cm spacer	Air	Small shipping can
88	Br-82	0.58	0.62	1.07	5.5 cm spacer	Air	Small shipping can
88	W-187	0.04	0.05	1.25	5.5 cm spacer	Air	Small shipping can
88	Mn-54	0.02	0.02	1.00	5.5 cm spacer	Air	Small shipping can
88	Mn-56	0.13	0.14	1.08	5.5 cm spacer	Air	Small shipping can
88	K-42	0.06	0.07	1.17	5.5 cm spacer	Air	Small shipping can
	Total	0.97	1.67	1.72			

continued on next page

continued from previous page

ID	Isotope	G2K	Eq. 2.4	Eq. 2.4/G2K	Position	Attenuator	Geometry
98	Na-24	1.04	0.46	0.44	5.5 cm spacer	Air	Small shipping can
98	Ar-41	0.87	0.39	0.45	5.5 cm spacer	Air	Small shipping can
98	Mn-56	1.54	0.69	0.45	5.5 cm spacer	Air	Small shipping can
98	Br-82	0.30	0.13	0.43	5.5 cm spacer	Air	Small shipping can
	Total	3.76	1.67	0.44			
97	Na-24	18.62	39.24	2.11	Top shelf lead cave	Water Marinelli	Small shipping can
97	Ar-41	3.50	0	∞	Top shelf lead cave	Water Marinelli	Small shipping can
97	Mn-56	6.85	0.07	0.01	Top shelf lead cave	Water Marinelli	Small shipping can
97	Br-82	1.70	3.35	1.97	Top shelf lead cave	Water Marinelli	Small shipping can
97	Sb-122	0.47	2.34	4.98	Top shelf lead cave	Water Marinelli	Small shipping can
	Total	31.14	45.00	1.45			
93	Sc-46	0.12	0.11	0.92	0.5 cm spacer	Air	Small shipping can

continued on next page

continued from previous page

ID	Isotope	G2K	Eq. 2.4	Eq. 2.4/G2K	Position	Attenuator	Geometry
93	Cr-51	0.07	0.06	0.86	0.5 cm spacer	Air	Small shipping can
93	Mn-54	0.23	0.02	0.09	0.5 cm spacer	Air	Small shipping can
93	Co-60	0.06	0.05	0.83	0.5 cm spacer	Air	Small shipping can
93	Fe-59	0.15	0.13	0.87	0.5 cm spacer	Air	Small shipping can
93	Cd-109	0.16	0.14	1.40	0.5 cm spacer	Air	Small shipping can
93	Ba-131	0.11	0.09	0.82	0.5 cm spacer	Air	Small shipping can
93	La-140	0.07	0.06	0.86	0.5 cm spacer	Air	Small shipping can
	Total	0.97	0.66	0.68			
90	Na-24	5.89	10.49	1.78	Well lead cave	Air	Small shipping can
90	Ar-41	8.27	14.71	1.78	Well lead cave	Air	Small shipping can
90	K-42	0.16	0.28	1.75	Well lead cave	Air	Small shipping can
90	Mn-56	5.50	9.79	1.78	Well lead cave	Air	Small shipping can
90	Br-82	1.71	3.06	1.79	Well lead cave	Air	Small shipping can
	Total	21.53	38.33	1.78			

continued on next page

continued from previous page

ID	Isotope	G2K	Eq. 2.4	Eq. 2.4/G2K	Position	Attenuator	Geometry
99	Na-24	4.76	9.50	2.00	Middle shelf lead cave	Air	Small shipping can
99	Cl-38	4.19	8.38	2.00	Middle shelf lead cave	Air	Small shipping can
99	Ar-41	8.09	16.18	2.00	Middle shelf lead cave	Air	Small shipping can
99	Mn-56	3.84	7.68	2.00	Middle shelf lead cave	Air	Small shipping can
99	Br-82	1.63	3.26	2.00	Middle shelf lead cave	Air	Small shipping can
	Total	22.51	45.00	2.00			
100	Sc-46	0.39	0.96	2.45	Middle shelf lead cave	Air	Small shipping can
100	Cr-51	26.39	64.08	2.43	Middle shelf lead cave	Air	Small shipping can
100	Mn-54	1.29	3.15	2.44	Middle shelf lead cave	Air	Small shipping can
100	Fe-59	13.33	32.55	2.44	Middle shelf lead cave	Air	Small shipping can
100	Co-60	1.91	4.67	2.44	Middle shelf lead cave	Air	Small shipping can
100	Zn-65	20.81	50.83	2.44	Middle shelf lead cave	Air	Small shipping can
100	Ru-103	0.53	1.30	2.44	Middle shelf lead cave	Air	Small shipping can

continued on next page

continued from previous page

ID	Isotope	G2K	Eq. 2.4	Eq. 2.4/G2K	Position	Attenuator	Geometry
100	Cs-134	0.33	0.80	2.46	Middle shelf lead cave	Air	Small shipping can
	Total	64.98	158.34	2.44			
101	Na-24	1.86	4.66	2.51	Middle shelf lead cave	Air	Small shipping can
101	Ar-41	2.65	6.65	2.51	Middle shelf lead cave	Air	Small shipping can
101	Mn-56	2.21	5.55	2.51	Middle shelf lead cave	Air	Small shipping can
101	Br-82	1.07	2.68	2.51	Middle shelf lead cave	Air	Small shipping can
101	W-187	0.09	0.22	2.53	Middle shelf lead cave	Air	Small shipping can
101	K-42	0.08	0.20	2.57	Middle shelf lead cave	Air	Small shipping can
101	Mn-54	0.02	0.05	2.45	Middle shelf lead cave	Air	Small shipping can
	Total	7.97	20.01	2.51			
102	Na-24	4.52	8.75	1.94	Middle shelf lead cave	Air	Small shipping can
102	Cl-38	4.69	7.93	1.69	Middle shelf lead cave	Air	Small shipping can

continued on next page

continued from previous page

ID	Isotope	G2K	Eq. 2.4	Eq. 2.4/G2K	Position	Attenuator	Geometry
102	Ar-41	6.81	11.50	1.69	Middle shelf lead cave	Air	Small shipping can
102	Mn-56	6.78	11.46	1.69	Middle shelf lead cave	Air	Small shipping can
102	Br-82	1.20	2.03	1.69	Middle shelf lead cave	Air	Small shipping can
	Total	23.99	41.67	1.74			
103	Na-24	2.82	2.33	0.83	Middle shelf lead cave	Air	Small shipping can
103	Cl-38	4.98	4.11	0.82	Middle shelf lead cave	Air	Small shipping can
103	Ar-41	4.60	3.80	0.83	Middle shelf lead cave	Air	Small shipping can
103	Mn-56	7.31	6.04	0.83	Middle shelf lead cave	Air	Small shipping can
103	Br-82	2.42	2.00	0.83	Middle shelf lead cave	Air	Small shipping can
103	Mn-54	0.06	0.05	0.87	Middle shelf lead cave	Air	Small shipping can
	Total	22.20	18.33	0.83			
104	Na-24	4.90	5.36	1.09	Middle shelf lead cave	Air	Small shipping can
104	Cl-38	5.23	5.72	1.09	Middle shelf lead cave	Air	Small shipping can

continued on next page

continued from previous page

ID	Isotope	G2K	Eq. 2.4	Eq. 2.4/G2K	Position	Attenuator	Geometry
104	Ar-41	9.68	10.60	1.10	Middle shelf lead cave	Air	Small shipping can
104	Mn-56	3.61	3.95	1.09	Middle shelf lead cave	Air	Small shipping can
104	Br-82	1.50	1.64	1.09	Middle shelf lead cave	Air	Small shipping can
104	k-42	0.29	0.32	1.10	Middle shelf lead cave	Air	Small shipping can
104	Ba-139	0.67	0.73	1.09	Middle shelf lead cave	Air	Small shipping can
	Total	25.89	28.32	1.09			
105	Na-24	3.88	6.41	1.65	Well	Air	Small shipping can
105	Cl-38	2.20	3.63	1.65	Well	Air	Small shipping can
105	Ar-41	4.04	6.60	1.63	Well	Air	Small shipping can
105	K-42	0.06	0.10	1.70	Well	Air	Small shipping can
105	Mn-56	6.98	11.53	1.65	Well	Air	Small shipping can
105	Br-82	1.05	1.73	1.64	Well	Air	Small shipping can
	Total	18.22	30.00	1.65			

continued on next page

continued from previous page

ID	Isotope	G2K	Eq. 2.4	Eq. 2.4/G2K	Position	Attenuator	Geometry
106	Sc-46	73.17	116.61	1.59	Corner	Air	Small shipping can
106	Sb-122	45.32	72.20	1.59	Corner	Air	Small shipping can
106	Fe-59	40.09	63.90	1.59	Corner	Air	Small shipping can
106	Cr-51	39.43	62.80	1.59	Corner	Air	Small shipping can
106	Co-60	19.48	31.03	1.59	Corner	Air	Small shipping can
106	Mn-54	5.51	8.79	1.59	Corner	Air	Small shipping can
106	Zn-65	4.36	6.94	1.59	Corner	Air	Small shipping can
106	Ru-103	2.76	4.40	1.59	Corner	Air	Small shipping can
	Total	230.11	366.67	1.59			
108	Na-24	347.25	52.60	0.15	Middle shelf lead cave	Water Marinelli	Small shipping can
108	Br-82	4.14	0.63	0.15	Middle shelf lead cave	Water Marinelli	Small shipping can
108	Sb-122	0.73	0.11	0.15	Middle shelf lead cave	Water Marinelli	Small shipping can
	Total	352.12	53.34	0.15			

continued on next page

continued from previous page

ID	Isotope	G2K	Eq. 2.4	Eq. 2.4/G2K	Position	Attenuator	Geometry
109	Sc-46	0.18	0.34	1.90	5.5 cm spacer	Air	Small shipping can
109	Fe-59	0.15	0.29	1.89	5.5 cm spacer	Air	Small shipping can
109	Sb-122	0.25	0.48	1.90	5.5 cm spacer	Air	Small shipping can
109	K-40	0.06	0.11	1.84	5.5 cm spacer	Air	Small shipping can
109	Cr-51	0.08	0.15	1.87	5.5 cm spacer	Air	Small shipping can
109	Co-60	0.07	0.13	1.86	5.5 cm spacer	Air	Small shipping can
109	Ru-103	0.06	0.12	1.91	5.5 cm spacer	Air	Small shipping can
109	La-140	0.02	0.04	1.98	5.5 cm spacer	Air	Small shipping can
	Total	0.88	1.66	1.89			
110	Na-24	313.35	56.33	0.18	Middle shelf lead cave	Air	Small shipping can
110	Br-82	1.86	0.33	0.18	Middle shelf lead cave	Air	Small shipping can
	Total	315.21	56.66	0.18			
111	Cr-51	1.86	0.1	0.05	0.5 cm spacer	Air	Small shipping can

continued on next page

continued from previous page

ID	Isotope	G2K	Eq. 2.4	Eq. 2.4/G2K	Position	Attenuator	Geometry
111	Mn-54	0.45	0.02	0.04	0.5 cm spacer	Air	Small shipping can
111	Sc-46	0.22	0.01	0.05	0.5 cm spacer	Air	Small shipping can
111	Fe-59	0.27	0.02	0.07	0.5 cm spacer	Air	Small shipping can
	Total	2.80	0.15	0.05			
113	Na-24	14.55	1.29	0.09	5.5 cm spacer	Air	Small shipping can
113	K-42	2.11	0.19	0.09	5.5 cm spacer	Air	Small shipping can
113	Br-82	2.14	0.19	0.09	5.5 cm spacer	Air	Small shipping can
	Total	18.80	1.67	0.09			
114	Cr-51	1.39	0.99	0.71	0.5 cm spacer	Air	Small shipping can
114	Mn-54	0.11	0.08	0.72	0.5 cm spacer	Air	Small shipping can
114	Zn-65	0.11	0.08	0.74	0.5 cm spacer	Air	Small shipping can
114	Mo-99	0.13	0.09	0.68	0.5 cm spacer	Air	Small shipping can
114	Sb-122	2.80	1.99	0.71	0.5 cm spacer	Air	Small shipping can

continued on next page

continued from previous page

ID	Isotope	G2K	Eq. 2.4	Eq. 2.4/G2K	Position	Attenuator	Geometry
114	Co-58	0.07	0.05	0.76	0.5 cm spacer	Air	Small shipping can
114	Fe-59	0.01	0.05	7.56	0.5 cm spacer	Air	Small shipping can
114	Sc-46	0.02	0.02	0.84	0.5 cm spacer	Air	Small shipping can
	Total	4.64	3.35	0.72			
117	Na-24	56.02	7.58	0.14	5.5 cm spacer	Air	Small shipping can
117	K-42	4.31	0.58	0.13	5.5 cm spacer	Air	Small shipping can
117	Br-82	2.50	0.34	0.14	5.5 cm spacer	Air	Small shipping can
117	Sb-122	0.99	0.13	0.13	5.5 cm spacer	Air	Small shipping can
117	Sb-124	0.01	0.00	0.00	5.5 cm spacer	Air	Small shipping can
117	W-187	34.75	4.70	0.14	5.5 cm spacer	Air	Small shipping can
	Total	98.59	13.33	0.14			
